Received: 5 May 2021 | Accepted: 10 January 2022

DOI: 10.1002/agg2.20247

Agrosystems, Geosciences & Environment OPEN ACCESS

ORIGINAL RESEARCH ARTICLE

Agrosystems

Assessment of cotton and sorghum stand establishment using UAV-based multispectral and DSLR-based RGB imagery

Madhav Dhakal[1,5] | **Yanbo Huang**[2] | **Martin A. Locke**[1] | **Krishna N. Reddy**[2] | **Matthew T Moore**[1] | **L. Jason Krutz**[3] | **Drew Gholson**[4] | **Rajen Bajgain**[1,6]

[1] USDA-ARS, National Sedimentation Laboratory, Oxford, MS 38655, USA

[2] USDA-ARS, Crop Production Systems Res. Unit, Stoneville, MS 38776, USA

[3] Mississippi Water Resources Research Institute, Mississippi State Univ., Mississippi State, MS 39762, USA

[4] Delta Research and Extension Center, Stoneville, MS 38776, USA

[5] Rodale Institute, Kutztown, PA 19530, USA

[6] Arable Labs Inc., 51 Federal St, Suite 301, San Francisco, CA 94107, USA

Correspondence
Madhav Dhakal, Rodale Institute, Kutztown, PA, USA.
Email: madhav.dhakal@rodaleinstitute.org

Assigned to Associate Editor Jodie McVane Reisner.

Abstract

Plant density and canopy cover are key agronomic traits for cotton (*Gossypium hirsutum* L.) and sorghum [*Sorghum bicolor* (L.) Moench] phenotypic evaluation. The objective of this study was to evaluate utility of broadband red–green–blue (RGB) and narrowband green, red, red-edge, and near-infrared spectral data taken by an unmanned aerial vehicle (UAV), and RGB taken by a digital single-lens reflex camera for assessing the cotton and sorghum stands. Support Vector Machine was used to analyze UAV images, whereas ImageJ was used for RGB images. Fifteen vegetation indices (VIs) were evaluated for their accuracy, predictability, and residual yield. All VIs had Cohen's $k > .65$, F score $> .63$, and User and Producer accuracy of more than 71 and 69%, respectively. Soil-adjusted vegetation indices (SAVIs) among narrowband VIs and excess green minus excess red (ExG–ExR) among broadband VIs provided more agreeable estimates of cotton and sorghum density than the remaining VIs with R^2 and index of agreement (IoA) up to .79 and .92, respectively. The estimated canopy cover explained up to 83 and 82% variability in leaf area index (LAI) of cotton and sorghum, respectively. The ImageJ produced R^2 from .79 to .90 and .83 to .86 and IoA .89 to .97 and ∼.91 between estimated and observed cotton and sorghum density, respectively. ImageJ explained up to 82 and 79% variability in cotton and sorghum LAI, respectively. Although ImageJ can give close estimates of crop density and cover, UAV-based narrowband VIs still can provide an agreeable, reliable, and time-efficient estimate of these attributes.

Abbreviations: CC, cover cropping; CI_{RE}, red-edge chlorophyll index; CT, conventionally tilled; DSLR, digital single-lens reflex camera; EDM, Euclidean distance map; ExR, excess red; ExG–ExR, excess green minus excess red; IoA, index of agreement; LAI, leaf area index; LTAR, long-term agroecosystem research; MAE, mean absolute error; MSAVI, modified soil adjusted vegetation index; NC, no-cover cropping; NGDRI, normalized green red difference index; NIR, near-infrared; NT, no-till; OBIA, object-based image classification; OSAVI, optimized soil adjusted vegetation index; PA, producer accuracy; RE, red-edge; RE–R, red-edge minus red; RMSE, root mean square error; ROI, region of interest; SEE, standard error of estimate; SVM, support vector machine; TVI, triangular vegetation index; UA, user accuracy; UAV, unmanned aerial vehicle; VI, vegetation index.

1 | INTRODUCTION

Assessment of crop stand establishment early in the season may allow us to evaluate planter performance, assess operator performance, map soil spatial variability, identify biotic and abiotic stressors, and predict crop yield and economic return. Estimating green canopy cover and plant density at early stages is crucial for precision agronomic applications such as variable-rate fertilization and irrigation (Ferguson & Rundquist, 2018). Achieving desirable plant density is often challenging, as management factors such as tillage and surface cover management, fertilization, irrigation, and weed management may influence seedling emergence and establishment. Plant density also drives vegetative surface cover or green cover, as viewed from a nadir position, enabling one to detect variability in crop growth and monitor physiological stressors.

Traditionally, plant density is assessed manually by counting seedlings (Dhakal et al., 2019), which is time consuming and laborious and may not represent large areas with high variability. Also, manual estimations are subjective, and visual assessments vary among observers (Duan et al., 2017). Indirect assessment (e.g., remote sensing or proximal sensing) may overcome these challenges. Unmanned aerial vehicles (UAV) have become more widely used for autonomous mission planning in precision agriculture (Duan et al., 2017; Li et al., 2020) as this method is completely nondestructive at all growth stages (Portz et al., 2012) and can be used under adverse field conditions with adjustable speeds (Chapman et al., 2014). Vegetation indices (VIs) calculated from UAV images demonstrated promising results in ground cover estimation and plant emergence for a variety of row crops (Chu et al., 2016; Duan et al., 2017; Jin et al., 2017; Koh et al., 2019; Li et al., 2019; Liu et al., 2017; Zhao et al., 2018).

Many studies rely on VIs as proxies of canopy attributes based on the broadband red–green–blue (RGB) spectrum (Koh et al., 2019; Li et al., 2019; Li et al., 2020; Zhao et al., 2018). A few studies showed narrowband VIs providing slightly better estimates of crop attributes than broadband VIs (Thenkabail et al., 2000; Zhao et al., 2007). Broadband- and narrowband-based VIs were compared for crop phenotyping using either satellite imagery (Thenkabail et al., 2002) or near-surface sensing platforms (Broge & Mortensen, 2002; Zhao et al., 2007), but there is limited information on the prediction of the canopy area and plant density, specifically for grain sorghum [*Sorghum bicolor* (L.) Moench] and cotton (*Gossypium hirsutum* L.).

High-resolution RGB images from a digital single-lens-reflex (DSLR) camera have been effectively used for ground cover estimation by classifying and separating plant pixels from the background (Baxter et al., 2017; Xiong et al., 2019). Baxter et al. (2017) and Xiong et al. (2019) used open-source software ImageJ (https://imagej.net/) for RGB image processing. This method may enable us to validate remote sensing results, although all methods require multiple comparisons with ground-truth data such as stand count and leaf area index (LAI).

Core ideas

- Utility of unmanned aerial vehicle-based multispectral imagery was compared with ImageJ-based red–green–blue analysis.
- Five vegetation indices in broadband and 10 in narrowband spectra were evaluated.
- Soil line narrowband indices improved predictability and accuracy of stand assessment.
- ImageJ provided a better estimation of plant density and leaf area index than an unmanned aerial vehicle-based method.

Adoption of UAV technology in agricultural production systems can speed up image acquisition and pre-processing since these methods integrate robotic operations and machine vision (Duan et al., 2017). This technology has been limited by lack of information on appropriate tools and procedures (Czarnecki et al., 2017), and the value and utility of this tool has not reached growers' level. Our study pursued using an open-source vs. commercial imagery processing tool with intent to provide a detailed approach and investigate reliability of various methods in characterizing plant attributes in the early vegetative growth stage. Specific objectives were to (a) compare VIs derived from broadband and narrowband spectral data in estimating plant density and LAI of cotton and sorghum, (b) evaluate UAV-based multispectral image analysis and DSLR-based RGB image analysis for crop stand assessment, and (c) confirm the usability of selected methods with datasets obtained from an independently designed experiment.

2 | MATERIALS AND METHODS

2.1 | Experimental site

The study consisted of two research areas. One research area (site long-term agroecosystem research [LTAR], 1.5 ha, 33.442279 °N, –90.885838 °W; 38 m asl) was utilized for the comparison of management practices, assessment methods, and VIs, and to define relationships between estimated and actual values. The second research area (site 21-Gun, 2.7 ha, 33.418012 °N, –90.898855 °W; 37 m asl) was used to test

validity of the generated relations and selected best models. These two sites were located 1.6-km apart in Stoneville, MS.

2.2 | Experimental design

2.2.1 | Evaluation: LTAR site

Twelve treatments, comprising a factorial of three crop rotations (monoculture sorghum [*Sorghum bicolor* L. Moench], monoculture cotton [*Gossypium hirsutum* L.], and cotton–sorghum rotation) × two cover crop treatments (no cover and cover [Austrian winter pea, *Pisum sativum* L.]) × two tillage systems (tillage and no-tillage), were laid out in a randomized complete block design with four replications. Individual plot sizes were 33.5 × 8 m, with eight 1-m wide crop rows. Austrian pea was terminated with paraquat (1.1 kg a.i. ha^{-1}) about 2 wk prior to planting. On 17 May 2019 and 13 May 2020, a 4-m-wide tractor-mounted planter was used to plant cotton (Phytogen 430 W3FE) and grain sorghum (Pioneer 84P80) (seeding rate 56 and 78 kg ha^{-1}, respectively). Fertilizer application, insect control, and preemergence and postemergence herbicide programs were standard for both cotton and sorghum. Crops were irrigated as needed.

2.2.2 | Validation: 21-Gun site

This second study was conducted to test the usefulness of VIs selected at the first (LTAR) site as there was potential that those indices could be affected by crop status, surface characteristics, and UAV's flight paths. In May 2020, after winter vegetation was burned down with herbicide, the entire study area was tilled and precisely leveled, and a new experimental design was installed with 21 plots. Plot dimensions were 152 m long ×8 m wide (eight 1-m wide rows on raised seedbeds), and plots were separated by 2-m-wide levees. Cotton cultivar Deltapine 2020 B3XF was planted on 1 June 2020 (113,668 seeds ha^{-1} to achieve a density of 75,000 plants ha^{-1}). All 21 plots were used for evaluation purposes since this was an establishment year, and all plots had the same agronomic management.

2.3 | Image acquisition and processing

2.3.1 | Unmanned aerial vehicle image acquisition and processing

Images were acquired using two quadcopter UAVs (DJI Phantom 3 Pro and a DJI Phantom 3 Advanced, DJI Technology Co.), each of which was mounted with a portable Parrot Sequoia multispectral camera (Parrot). The camera used for imaging had a sensor to capture broadband RGB (14 MP), and narrowband red (660 nm, ± 40 nm), green (550 nm, ± 40 nm), red-edge (735 nm, ± 10 nm), and near-infrared (NIR) (790 nm, ± 40 nm) wavelengths, respectively. The sensor automatically corrected brightness and synchronized GPS positions with UAV. The UAV flights were operated above cotton and sorghum plots between 10:30 a.m. and 12:00 p.m. CST as weather permitted, with flight altitude 60 m above canopy surface. Flight routes were preset using DroneDeploy (DroneDeploy, Inc.) in 2019 and Pix4DCapture (Pix4D S.A.) in 2020. Table 1 shows records of UAV image acquisitions for the two fields.

Of the approximately 500 images captured with flight about 350 images were finally used for further processing. Images were imported to Pix4DMapper 4.2 (Pix4D S.A.) to generate RGB orthomosaic in broadband and red, green, red-edge, and NIR orthomosaics in narrowband spectrum, which were orthorectified to correct geometric and vignetting distortion.

Orthomosaic images were imported to ArcGIS Pro (ESRI) for further processing (Figure 1). The visual boundary of each image was used to draw a shapefile to examine dimension and area for each plot, and Python script (Python Software Foundation) was written (Zandbergen, 2013) to focus on areas of interest. A classification schema was created for plant and bare surfaces. An initial segmented raster dataset was created as an input to reference the existing dataset before training the classifier, and training samples were generated with respect to the segmented image, corresponding to the classification schema. More than 20 and 50% pixels were picked to train the sample for plant and bare surface classes, respectively, to ensure statistical significance for reliable classification. A reference dataset was provided to assess accuracy of classified results.

Spectral and spatial details were provided based on crop species to be segmented. Minimum segment size was determined based on actual plant leaf area. Before running samples in batch, "segmented boundaries" and "number of segments overlaid on the source images" were evaluated and compared by dynamically rerunning the segmentation via changing the parameters. A highly advanced nonparametric machine learning classifier called support vector machine (SVM) (Vapnik, 2013) was used to train samples.

After classifying images with SVM, results were compared with reference datasets for accuracy assessment by creating more than 500 random points. Cohen's kappa coefficient (k) (McHugh, 2012) and F score (Sasaki, 2007) were assessed to analyze accuracy of results. These accuracy ratings ranged from 0 to 1, with 1 being 100% accurate. Cohen's k coefficient can be written as Equation 1 (McHugh, 2012):

$$k = 1 - \frac{1 - p_o}{p_e} \quad (1)$$

TABLE 1 Date, unmanned aerial vehicle (UAV) model, site, and weather conditions during UAV imagery time

Date	UAV	Field	Weather
12 June 2019	DJI Phantom 3 Advanced	LTAR	Mostly overcast
12 June 2020	DJI Phantom 3 Pro	LTAR	Sunny clear
20 June 2020	DJI Phantom 3 Advanced	21-Gun	Mostly sunny

Note. LTAR, long-term agroecosystem research.

where p_o is relative observed agreement between raster images, and p_e is hypothetical probability of agreement. The confusion matrix obtained from accuracy assessment also includes F score (or Sorensen–Dice coefficient), which can be defined as Equation 2 (Sasaki, 2007):

$$F1 = 2\frac{\text{precision}\,(\text{recall})}{\text{precision} + \text{recall}} \quad (2)$$

where precision = TP/(TP + FP) and recall = TP/(TP + FN), TP = true positive or extracted pixel representing plant in the reference, FP = false positive or extracted pixel represents plant pixels not in the reference, and FN = false negative or extracted pixel does not represent true plant pixels.

For a few datasets, errors in classification results were minimized by using a "Reclassifier" tool, and changes were verified with source images. Denser and solid rows of sorghum caused by overlapping leaves created elongated objects that were often resistant to filter and rescaling functions. In that case, the raster dataset was split based on a pixel threshold per plant and feature attributes of classified segments. A lower threshold rescaling factor was applied to remove <10-pixel objects for broadband images and <1 pixel for narrowband images to filter unidentified objects. Number of pixels per object and per plant was determined by stratified random sampling. Area of crop and bare surface (m^2) were calculated for each plot. Plant density estimates were computed by summing all numbers of objects within each plot for each crop and extrapolated to per hectare basis for comparison. Objects having pixels more than two times greater than actual number of pixels per plant were considered outliers and removed during the regression procedure.

2.3.2 | Selection of vegetation indices and zonal statistics

Input variables for color object identification and segmentation utilized various VIs based on broadband RGB and narrowband green, red, red-edge, and NIR orthomosaic images (Table 2). Initially, 50 VIs commonly used by researchers were generated using map algebra and screened by testing segmentation accuracy and visualizing false-color composite. A single plot image was randomly sampled for each crop to test each VI, and VIs producing more than 50% user and

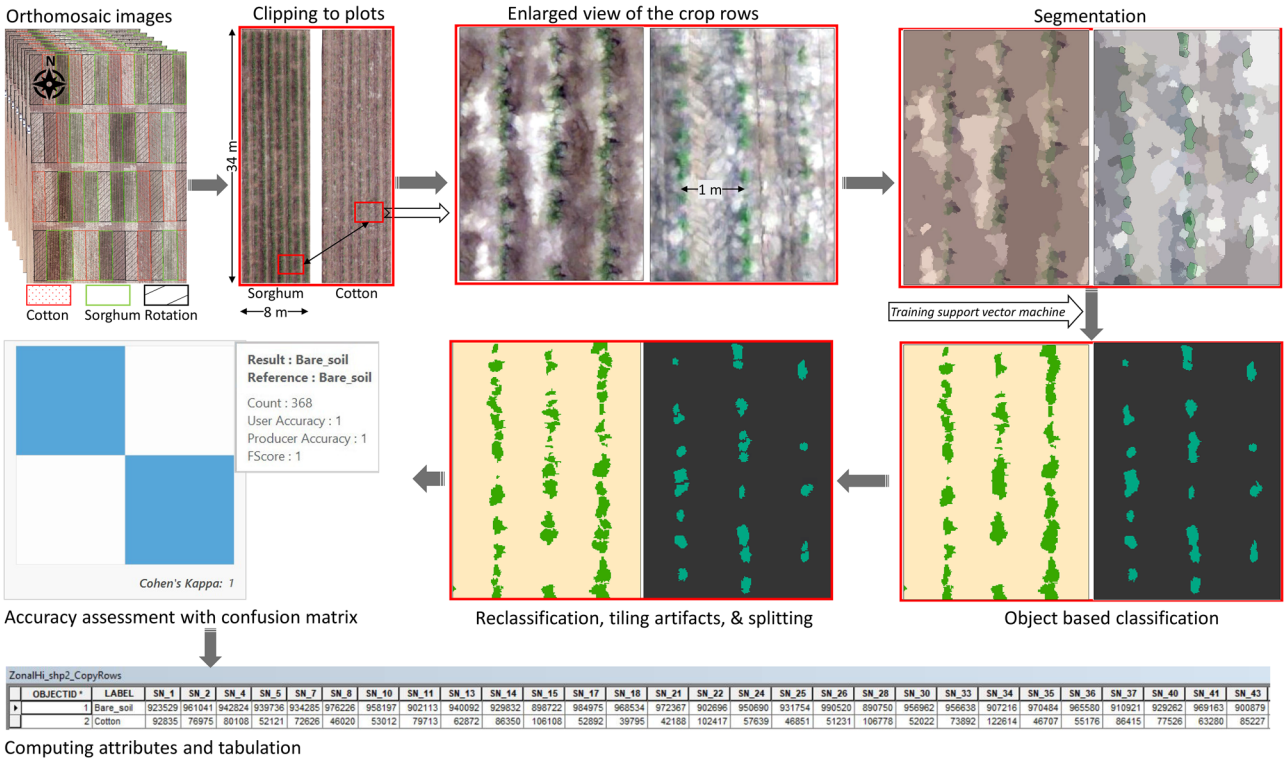

FIGURE 1 Diagram showing object-based image classification using support vector machine (SVM) in ArcGIS Pro. Image acquired on 12 June 2019

TABLE 2 Common vegetation indices based on broadband red–green–blue (RGB) and narrowband green, red, red-edge, and near-infrared (NIR) spectrum

Vegetation indices	Abbreviation	Equation	Reference
Broadband			
True color	RGB	–	–
Excess green index	ExG	2G – R – B	Jin et al. (2017); Li et al. (2019); Zhao et al. (2018)
Excess red index	ExR	1.4R – G	Jin et al. (2017); Zhao et al. (2018)
Excess green – excess red index	ExG – ExR	3G – 2.4R – B	Jin et al. (2017); Li et al. (2019); Zhao et al. (2018)
Normalized green – red difference index	NGRDI	(G–R)/(G+R)	Gitelson et al. (2002); Zhao et al. (2018)
Narrowband			
Wavelength of red-edge	RE	–	–
Wavelength of near-infrared	NIR	–	–
Red-edge minus red	rRE	RE – R	–
Wide dynamic range vegetation index	WDRVI	[(0.2 × NIR)–R]/[(0.2 × NIR) + R]	Gitelson (2004); Xue and Su (2017)
Triangular vegetation index	TVI	[(NIR–G) × 120] – [200 × (R – G)]/2	Broge and Leblanc (2000)
Red-edge chlorophyll index	CI_{RE}	(NIR/RE) – 1	Gitelson and Merzlyak (1994)
Two-band enhanced vegetation index	EVI2	2.5 × {(NIR–R)/[NIR + (2.4 × R) + 1]}	Jiang et al. (2008); Liu et al. (2012)
Soil adjusted vegetation index	SAVI	[(NIR–R)/(NIR + R + L)] (1 + L), $L = 0.90$	Huete (1988)
Modified soil adjusted vegetation index	MSAVI	$0.5 \times \{[2(NIR+1)] - \sqrt{(2 \times NIR+1)^2 - [8 \times (NIR - R)]}$	Qi et al. (1994)
Optimized soil adjusted vegetation index	OSAVI	(1 + 0.16) (NIR–R)]/(NIR +R + 0.16)	Haboudane et al. (2002); Rondeaux et al. (1996)

Note. R, red; G, green; B, blue; RE, red-edge.

producer accuracies were shortlisted for crop assessment. In addition to raster algebraic combination, true color composition of broadband RGB and wavelengths of dual-channel narrowband red-edge and NIR were also used for image segmentation. Overall, a total of 15 (5 broadband plus 10 narrowband) VIs were selected from the pool of 50 VIs. The VIs selected showed significant correlation at $\alpha \leq .05$ to canopy characteristics (Table 2). Zonal pixel values were recorded for each VIs in each band.

2.3.3 | DSLR image acquisition and processing with ImageJ

Canopy cover images were recorded using a Canon DSLR with EF 24–105 lens (Canon Inc.) from 1.5 m height. Photos were taken during the daytime on the same day as the UAV flights. A 1-m^2 PVC quadrat was placed on top of the ridge of the crop rows, parallel to the ground at three points within each plot. The camera was mounted on a 3-m long aluminum monopod to manually adjust for height by tilting and centering the camera over the quadrat. A remote controller was used to focus and capture images. A total of 144 images per plot were collected at each time.

Photographic images were cropped to the shape of a quadrat to represent a 1-m^2 area (Figure 2d and 2e) and imported to ImageJ (Version 1.38e) in Microsoft Java 1.1.4 platform. All images were run in a batch using unique macros for each sampling period; with separate batches prepared for cotton and sorghum and cover and no-cover crop plots (Figure 2d and 2e). A single reframed image from the batch was initially imported to determine threshold parameters in macros and adjust hue, saturation, brightness (HSB) for color thresholding. Binary grayscale images were created (Otsu thresholding algorithm) (Figure 2b and 2c), particles were removed (particle remover plugin) (Figure 2f and 2g), and size and circularity were modified to remove unwanted pixels. Particle size smaller than 300 pixels were removed with the circularity ranging from .001 to 1.00 (Figure 2j and 2k). Gaps between pixels and lost region of interest (ROI) were corrected with "fill holes"

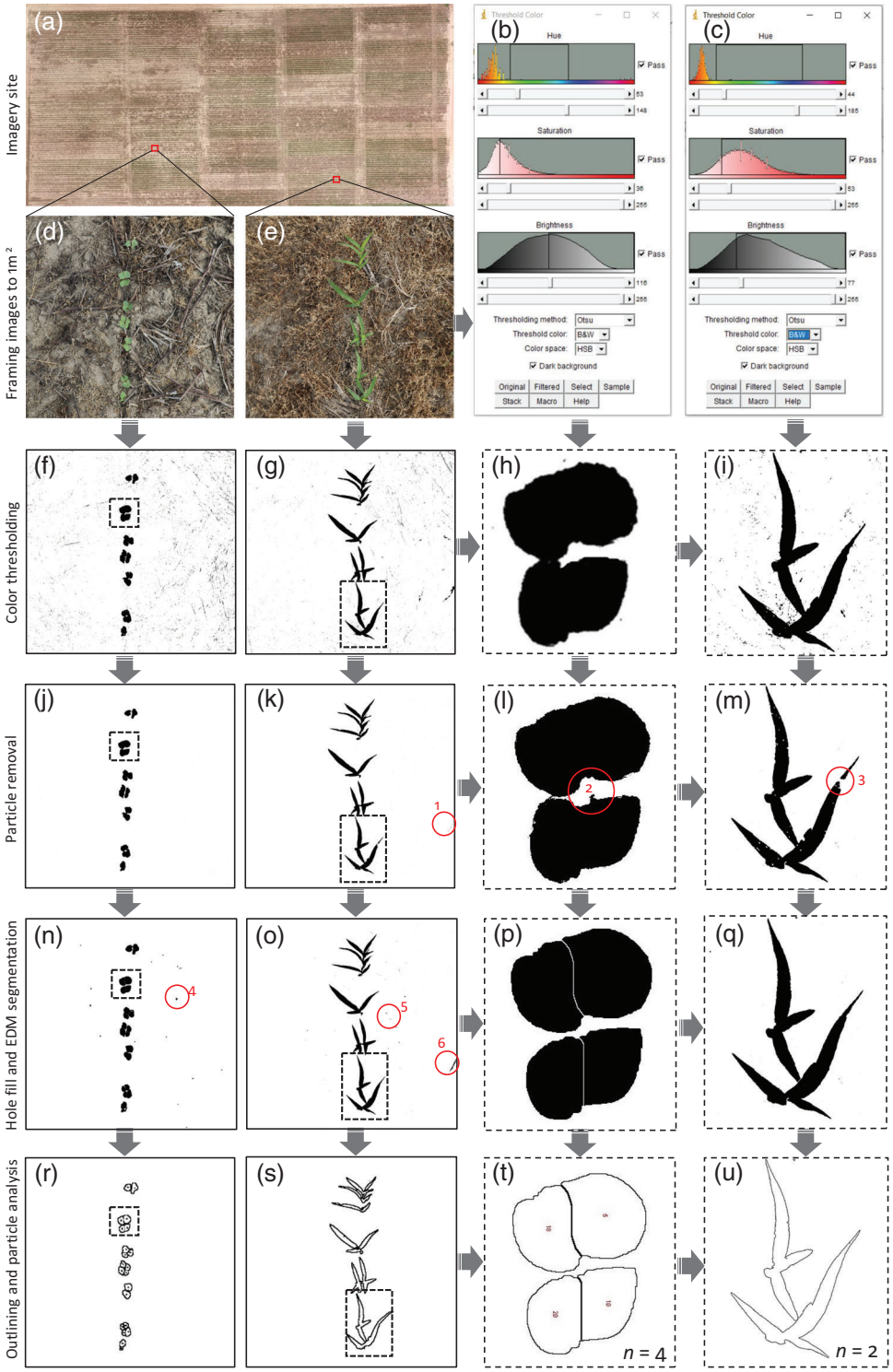

FIGURE 2 Schematic presentation of ImageJ data processing, (a) experiment plot, (b, c) hue, saturation, and brightness (HSB) thresholding platform, (f, g, h, i) segmented seedlings of cotton and sorghum, (j, k, l, m) corrected images after noise removal, (n, o, p, q) binary masked images after hole filling and dilation, (r, s, t, u) analyzed particles with region of interest (ROI) outlined. Red circle portrayed (1) oversized particles, (2, 3) lost ROI due to removal of particles, (4, 5, and 6) reappeared noise particles

and "dilate" options (Figure 2p and 2q). Corrected images were segmented by the Watershed segmentation tool. Cotton seedlings were in two- to three-leaf stage where top two leaves were in distinct positions (Figure 2l and 2p). This created two separate particles for a single plant before the binary image processing, whereas Euclidian distance map (EDM) segmentation further fragmented the particle into two halves from the midrib (Figure 2p). Midrib partition did not occur in sorghum as plant leaf characteristics were different from cotton, so two sets of macros were used for each crop. Segmented particles were analyzed for total count, size, and percentage area covered. Particle analysis process excluded edges of images, only including particles >1,000 pixels. Excluding edges removed the weed particle (red circles in Figure 2) from the images. Cotton produced two to four segments for each plant, so total number of segments was divided by number of segments per plant with the highest average probability ($P = .76$) obtained from the probability distribution curve. The average number of segments per cotton plant was three, which was used to calculate the adjusted cotton density in the ROI. For sorghum, each segment represented a single plant, thus the total count represented the number of plants m^{-2}.

2.4 | Ground data collection

Cotton and sorghum seedlings were counted 1 m row lengths for all crop rows in each plot on the same day UAV was deployed in both years. Plant density was calculated as the number of plants per hectare from the known length and row spacing. Five plants were randomly sampled in each plot to determine leaf area. Leaf area was determined by placing crop leaves on an area meter (LI-3100C, LI-COR, Inc.), and leaf area index (LAI) was calculated by dividing total leaf area by ground area.

2.5 | Data analysis

Analytical results from ArcGIS Pro and ImageJ and manually recorded plant density data were exported to Microsoft Excel for initial data visualization. Plant density data was right-skewed; thus, assumption of negative binomial distribution was made for that variable (Stroup, 2015). Plant density and percentage canopy cover were analyzed in SAS 9.4 (SAS Institute) using GLIMMIX procedure for comparing treatments within each year. Tillage and cover crop were set as fixed effects, whereas replication was set as a random effect. Means were separated using least significant difference (LSD) test at $\alpha = .05$. The relationship between actual and estimated data was analyzed by using PROC REG procedure in SAS. Pixel values for each band were regressed against crop LAI. Partial residual plots were analyzed to determine the linearity of the regression model. Influential outliers observed due to poor seedling emergence in some of the plots were removed based on studentized residuals and Cook's Distance at $\alpha = .05$ (Cook, 1977). Images from the LTAR site were used to evaluate the relationship between observed and estimated values, whereas data obtained from the 21-Gun site were used to evaluate consistency of the selected VIs and ImageJ in relation to the estimation of plant density and canopy cover in 2020. Coefficient of determination (R^2), root mean square error (RMSE), mean absolute error (MAE), and index of agreement (IoA) were computed to evaluate VIs and ImageJ performance. Both MAE and RMSE are similar measures, however, Willmott (1982) stressed that reporting both is more appropriate. The relationship between predicted and observed values was also expressed as an IoA.

3 | RESULTS

3.1 | Observed plant density and leaf area index

By design, sorghum had greater plant density than cotton in both years as the seeding rate was different (Table 3). Cotton emergence was greater in the 1st year (47,875 plants ha^{-1}) than in the 2nd year (71,000 plants ha^{-1}). Treatments had no effect on both cotton and sorghum density in 2019 ($P > .05$). In 2020, cover crop residue suppressed the cotton emergence, especially at no-till plots, relative to conventionally tilled residue-free plots ($P < .05$). A similar trend was observed for sorghum in 2020, where conventionally tilled (CT)–no-cover cropping (NC), that is, CT–NC had a higher sorghum density than no-till (NT) cover cropping (CC), that is, NT–CC ($P < .05$). Tillage and cover crop treatments had no effect on LAI of cotton and sorghum in 2019 ($P > .05$). In 2020, both NC treatment showed greater LAI than CC for both cotton and sorghum, especially in the no-tillage plots ($P < .05$).

3.2 | Zonal statistics and accuracy assessment of multispectral image analysis

Zonal statistics showed greater mean red reflectance in broadband from the cotton canopy than green and blue pixels (Figure 3a). Depressions in RGB values mostly occurred in sorghum plots. The pattern was similar for narrowband green, red, and red-edge (RE) reflectance (Figure 3b). Narrowband red, green, and RE wavelengths showed greater sensitivities with the changes in green cover than NIR. Pixel values for all broadband red, green, and blue and narrowband green and red were reduced with an increase in LAI, whereas RE and NIR had an opposite relationship. Red reflectance

TABLE 3 Plant density and leaf area index of cotton and sorghum in 2019 and 2020 at long-term agroecosystem research (LTAR) site, Stoneville, MS

	Plant density				Leaf area index			
	Cotton		Sorghum		Cotton		Sorghum	
Treatments	2019	2020	2019	2020	2019	2020	2019	2020
	plants ha^{-1}							
NT-NC	43,250	85,000a	84,000	84,250 ab	.34	.31ab	.75	.67b
NT-CC	50,750	48,000c	86,000	76,000 b	.35	.22b	.76	.55c
CT-NC	48,250	79,000 ab	87,000	98,250 a	.37	.35a	.84	.83a
CT-CC	49,250	72,000 b	83,500	85,250 ab	.36	.26ab	.75	.65 b
Tillage (T)	ns	*	ns	ns	ns	*	ns	**
Cover crop (C)	ns	*	ns	***	ns	***	ns	***
T × C	ns	**	ns	ns	ns	ns	***	ns

Note. CC, cover crop; CT, conventional tillage; NC, no cover crop; ns, not significant at the α = .05 level; NT, no tillage. Treatment means followed by the same lowercase letters are not different at α = .05.

*t test significant at α ≤ .05.

**t test significant at α ≤ .01.

***t test significant at α ≤ .001.

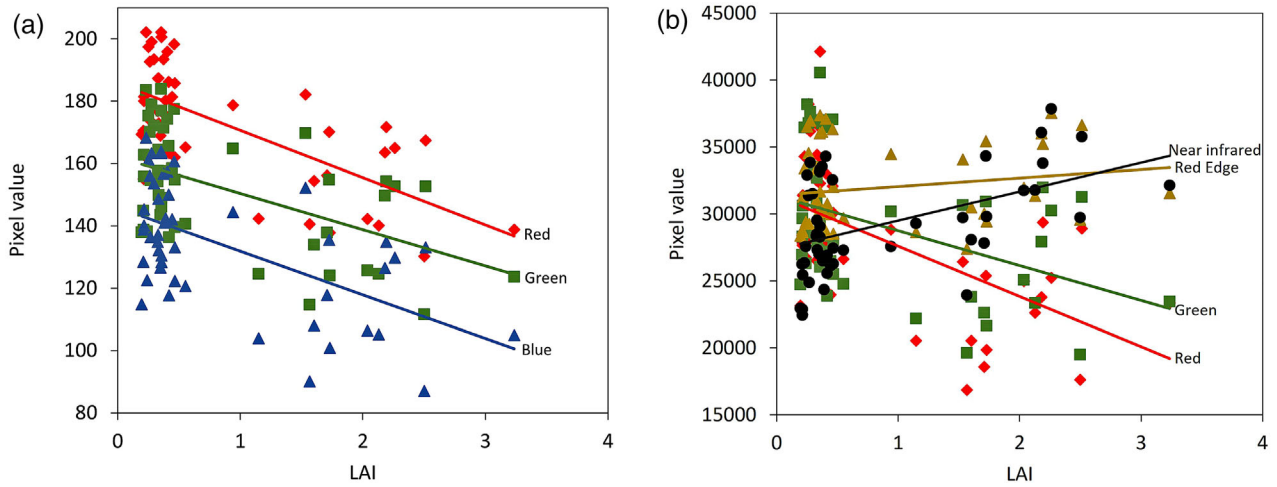

FIGURE 3 Linear relationships between pixel value and measured leaf area index (LAI) for (a) broadband and (b) narrowband spectrum. Data were averaged across the years and crops

exceeded NIR until the LAI reached .60 or for almost 80% of the plots at the time of data collection. This indicates dominance of soil and dead cover crop residue reflectance over greenness.

Segmentation accuracy was assessed for cotton and sorghum images (Figure 4), providing information on the degree to which the raster images were oversegmented or undersegmented. Ideally, a segmented image accurately resembles the reference surface where both user and producer accuracy would achieve 100% or 1. Undersegmented images show high producer accuracy and low user accuracy and vice-versa. Broadband VIs such as excess red (ExR), excess green minus excess red (ExG–ExR), and normalized green red difference index (NGDRI) and narrowband VIs such as near-infrared (NIR), triangular vegetation index (TVI), and red-edge minus red (RE–R) produced undersegmented raster images for cotton. Similarly, ExR and NGDRI among broadbands and NIR, two-banded enhanced vegetation index (EVI2), triangular vegetation index (TVI), and RE–R among narrowband indices produced undersegmented images for sorghum. The F score combined both user and producer accuracy, which was >90% for those images with narrowband indices: red-edge chlorophyll index (CI_{RE}), modified soil adjusted vegetation index (MSAVI), and RE–R for cotton and optimized soil adjusted vegetation index (OSAVI) for sorghum. None of the broadband indices produced more than 90% F score. The kappa value (k) was more than .90 with EVI2, MSAVI, TVI, and wide dynamic range vegetation

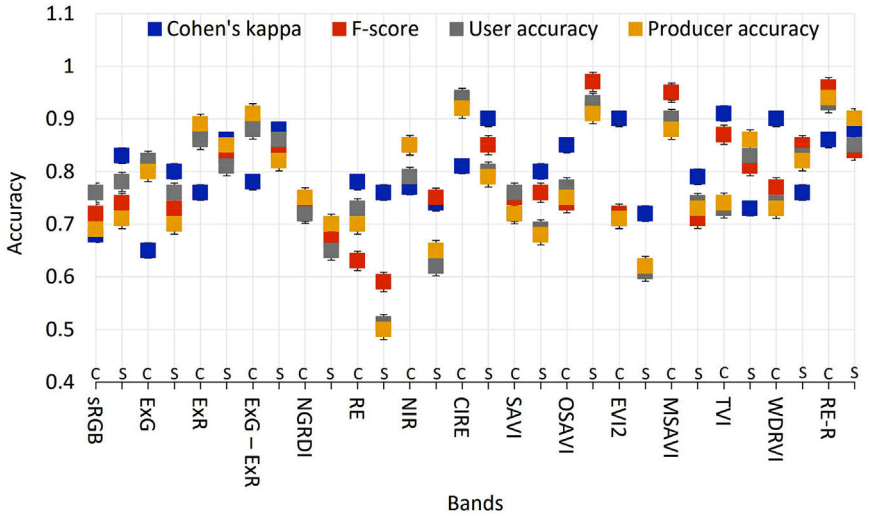

FIGURE 4 Accuracy assessment of segmentation for different vegetation indices (VIs) for cotton (C) and sorghum (S). Data were averaged across years, treatments, and replications. Broadband indices were RGB, red–green–blue; ExG, excess green; ExR, excess red; ExG–ExR, excess green minus excess red; NGRDI, normalized green red difference index; Narrowband indices were RE, wavelength of red-edge; NIR, wavelength of near-infrared; CI_{RE}, red-edge chlorophyll index; SAVI, soil adjusted vegetation index; OSAVI, optimized soil adjusted vegetation index; EVI2, two-band enhanced vegetation index; MSAVI, modified soil adjusted vegetation index; TVI, triangular vegetation index; WDRVI, wide dynamic range vegetation index; RE–R, red-edge minus red

index (WDRVI) for cotton, and CI_{RE}, MSAVI, and RE–R for sorghum. Among broadband indices, ExG–ExR showed the highest k and F score for both cotton and sorghum. Overall, ExG–ExR was effective among broadband VIs for both cotton and sorghum object segmentation, whereas MSAVI was effective for cotton and OSAVI for sorghum among narrowband VIs.

3.3 | Comparison of vegetation indices for plant density

Performance of each of the VIs was evaluated by comparing estimated vs. manually counted plant density at the early vegetative stage of the crop. In 2019, cotton density was effectively estimated by using narrowband indices with higher R^2 and IoA and lower RMSE and MAE than with broadband VIs (Table 4). Among broadband VIs, ExR had the lowest RMSE, MAE, and the highest IoA, although ExR overestimated cotton plant density below 50,000 plants ha^{-1}, but underestimated at dense areas (Figure 5). The ExG–ExR consistently overestimated plant density. The CI_{RE}, MSAVI, and RE–R among the narrowband indices produced R^2 >.70 and IoA more than .85 (Figure 6). All three VIs slightly underestimated cotton plant density below 50,000–60,000 plants ha^{-1} and overestimated density above that plant population range.

The RMSE and MAE estimations increased for most VIs in 2020 for cotton, whereas R^2 and IoA shifted within bandwidth groups as compared to 2019 (Table 4). For cotton, among broadband indices, true-color RGB showed the greatest R^2 and IoA compared with other Vis, but RGB underpredicted cotton density as compared with the observed density of cotton (Figure 5). In 2020, OSAVI and RE–R were the best-performing narrowband VIs, with more than .70 and .90 R^2 and IoA, respectively. Although OSAVI and RE–R were statistically more sound than other narrowband VIs, RE–R deviated slightly from the 1:1 line, underestimating cotton density in dense areas (Figure 6).

Broadband VIs ExR and ExG–ExR described 55% of variability in sorghum density in 2019 with RMSE and MAE approximately 10,000 and 8,000 plants ha^{-1}, respectively, and IoA close to .80 (Table 4). The regression lines for these indices were closer to the 1:1 line than other VIs (Figure 7). Among narrowband indices, OSAVI had the highest R^2 and IoA and the lowest RMSE and MAE, whereas CI_{RE}, TVI, and RE–R were intermediate between OSAVI and the remaining VIs. Although MSAVI had slightly lower R^2 than OSAVI and TVI, it was more proximate to the 1:1 line than TVI, whereas TVI overestimated the sorghum density below 85,000 plants ha^{-1} (Figure 8).

Estimating sorghum density from broadband VIs appeared to be ineffective in 2020 (Table 4), where all broadband VIs highly overestimated sorghum density, especially in low-density areas (Figure 7). Nevertheless, ExG–ExR was better among all broadband VIs with relatively higher R^2 and lower prediction errors. Narrowband VIs effectively segmented plant pixels from the bare soil and captured up to 70% variability in sorghum plant density, where OSAVI, MSAVI, and RE–R performed better than VIs not corrected for soil reflectance. The RE and WDRVI had lower and more inconsistent predictability as compared with the three above mentioned VIs. The RE–R, unlike soil adjusted indices, produced strong agreement between observed and estimated sorghum density in 2020 (Figure 8).

3.4 | Comparison of vegetation indices for canopy cover

Percentage canopy cover for cotton and sorghum was estimated using VIs in broadband and narrowband spectrum,

TABLE 4 Evaluation of vegetation indices (VIs) used to estimate plant density for cotton and sorghum with respect to the observed plant density in 2019 and 2020. The proportion of variance in predicted values is shown by R^2

Year	VIs	Cotton				Sorghum			
		R^2	RMSE	MAE	IoA	R^2	RMSE	MAE	IoA
			——plants ha^{-1}——				——plants ha^{-1}——		
2019	Broadband								
	RGB	.39	9,746	8,352	.75	.44	15,251	13,034	.72
	ExG	.35	10,588	8,858	.73	.37	28,999	23,934	.47
	ExR	.42	7,071	6,088	.80	.55	11,024	9,727	.82
	ExG–ExR	.58	9,733	7,792	.75	.55	10,813	8,464	.81
	NGRDI	.35	9,767	7,122	.70	.12	16,777	15,548	.56
	Narrowband								
	RE	.25	12,678	10,812	.62	.16	17,991	15,506	.58
	NIR	.67	8,754	7,553	.80	.43	17,915	15,638	.71
	CI_{RE}	.79	6,876	5,986	.90	.65	8,520	7,533	.88
	SAVI	.41	13,733	11,942	.70	.49	13,997	11,880	.77
	OSAVI	.48	14,673	12,084	.69	.73	6,946	6,025	.91
	EVI2	.43	16,453	14,816	.67	.35	11,372	10,008	.75
	MSAVI	.73	7,110	5,904	.88	.50	12,063	10,138	.80
	TVI	.63	8,568	6,983	.84	.67	7,907	6,623	.87
	WDRVI	.57	10,953	9,689	.75	.63	22,444	19,982	.63
	RE–R	.75	8,725	7,324	.85	.66	9,078	7,246	.87
2020	Broadband								
	RGB	.56	16,940	20,574	.76	.17	19,714	23,097	.63
	ExG	.46	16,119	18,474	.75	.35	16,882	19,227	.72
	ExR	.36	17,632	19,856	.72	.24	17,606	20,688	.62
	ExG–ExR	.22	17,469	19,876	.64	.40	16,830	19,073	.74
	NGRDI	.35	15,566	18,088	.75	.27	18,147	19,839	.68
	Narrowband								
	RE	.53	15,398	16,758	.84	.45	14,611	17,334	.74
	NIR	.63	11,705	13,220	.86	.65	14,979	17,172	.81
	CI_{RE}	.63	10,180	12,297	.88	.49	14,663	16,385	.79
	SAVI	.56	13,143	15,178	.82	.48	11,287	13,137	.77
	OSAVI	.70	9,750	11,033	.91	.71	13,110	15,854	.78
	EVI2	.59	12,103	14,022	.83	.52	10,611	13,040	.82
	MSAVI	.74	12,168	13,780	.90	.64	9,658	10,983	.88
	TVI	.56	11,901	13,728	.86	.52	13,490	14,766	.83
	WDRVI	.44	12,710	15,610	.79	.64	11,505	12,816	.87
	RE–R	.77	9,580	10,610	.92	.61	12,491	13,642	.90

Note. CI_{RE}, red-edge chlorophyll index; ExG, excess green; ExR, excess red; ExG–ExR, excess green minus excess red; EVI2, two-band enhanced vegetation index; IoA, index of agreement; MAE, mean absolute error; MSAVI, modified soil adjusted vegetation index; NGRDI, normalized green red difference index; NIR, wavelength of near infrared; OSAVI, optimized soil adjusted vegetation index; RE, wavelength of red-edge; RE–R, red-edge minus red; RGB, red–green–blue; RMSE, root mean square error; SAVI, soil adjusted vegetation index; TVI, triangular vegetation index; WDRVI, wide dynamic range vegetation index.

and its linear relationship to LAI (Table 5). Crops had more canopy cover in 2020 than 2019, with slightly greater variability among the VIs, especially with narrowband indices. Red-edge tended to have more canopy cover than others. The WDRVI had an estimate closer to observed values when averaged across the VIs within the broadband and narrowband VIs. The R^2 relating estimated canopy cover and LAI indicated greater predictability of ExG–ExR among broadband indices and MSAVI among narrowband indices for both crops (Table 5). Standard error of estimate (SEE) was <4.5 and 3.0% for sorghum and cotton, respectively (data not shown).

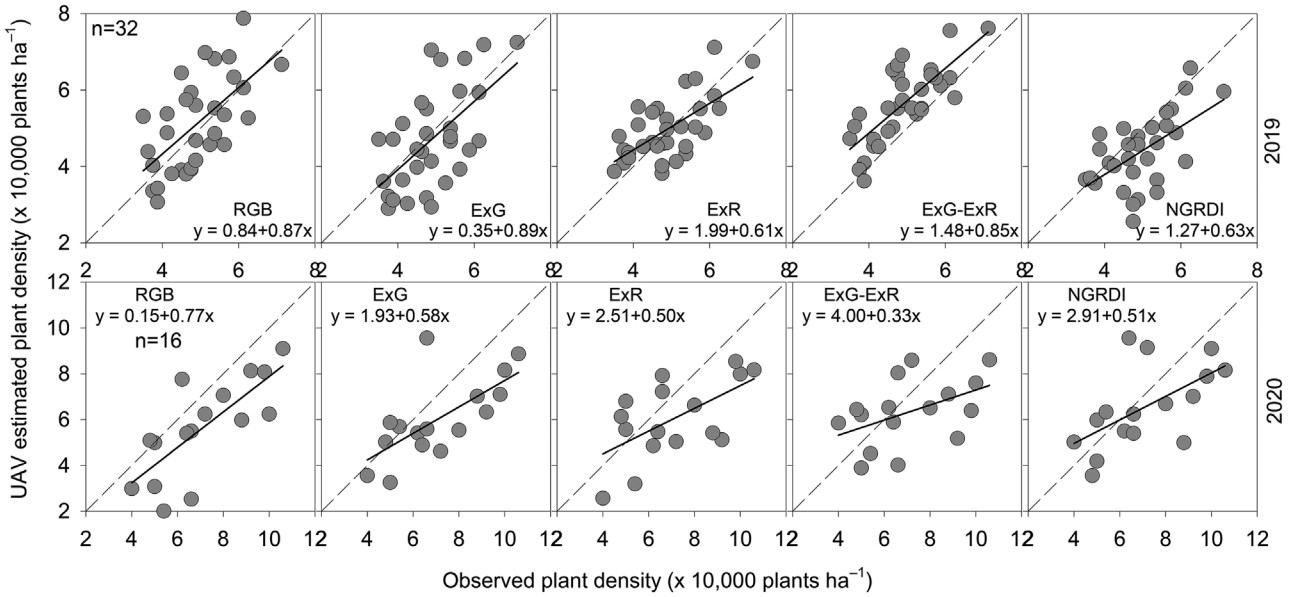

FIGURE 5 Relationship between observed and unmanned aerial vehicle (UAV) estimated cotton density in five broadband vegetation indices in (top) 2019 and (bottom) 2020. Vegetation indices are: RGB, red–green–blue; ExG, excess green; ExR, excess red; ExG–ExR, excess green minus excess red; NGRDI, normalized green-red difference index

3.5 | Performance of ImageJ based DSLR image analysis

ImageJ-based analysis showed promising predictions for both cotton and sorghum density and green cover in both years (Table 6). ImageJ produced RMSE and MAE lower than UAV methods with much stronger linear relation and IoA when comparing estimated plant density with observed density (Table 7). Slopes were equal to 1.0 in both 2019 ($P = .07$) and 2020 ($P = .21$) for both cotton and sorghum (Figure 9). Canopy cover estimated using ImageJ was linearly related to LAI ($P < .05$, Figure 9). Regression showed that sorghum maintained a similar LAI with largely varied canopy cover for both years. The SEE of the regressions was lower in cotton than in sorghum. Overall, ImageJ produced lower SEE of the estimation than that of using the UAV-based multispectral method.

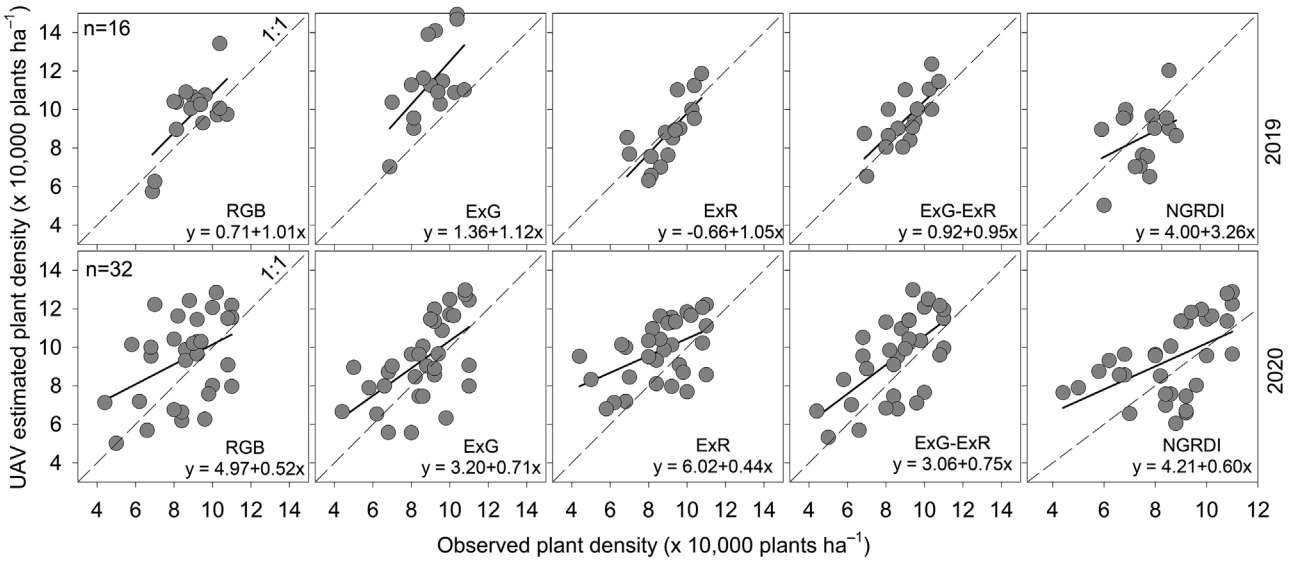

FIGURE 7 Relationship between observed and unmanned aerial vehicle (UAV) estimated plant density of sorghum in five broadband vegetation indices in (top) 2019 and (bottom) 2020. Vegetation indices: RGB, red–green–blue; ExG, excess green; ExR, excess red; ExG–ExR, excess green minus excess red; NGRDI, normalized green-red difference index

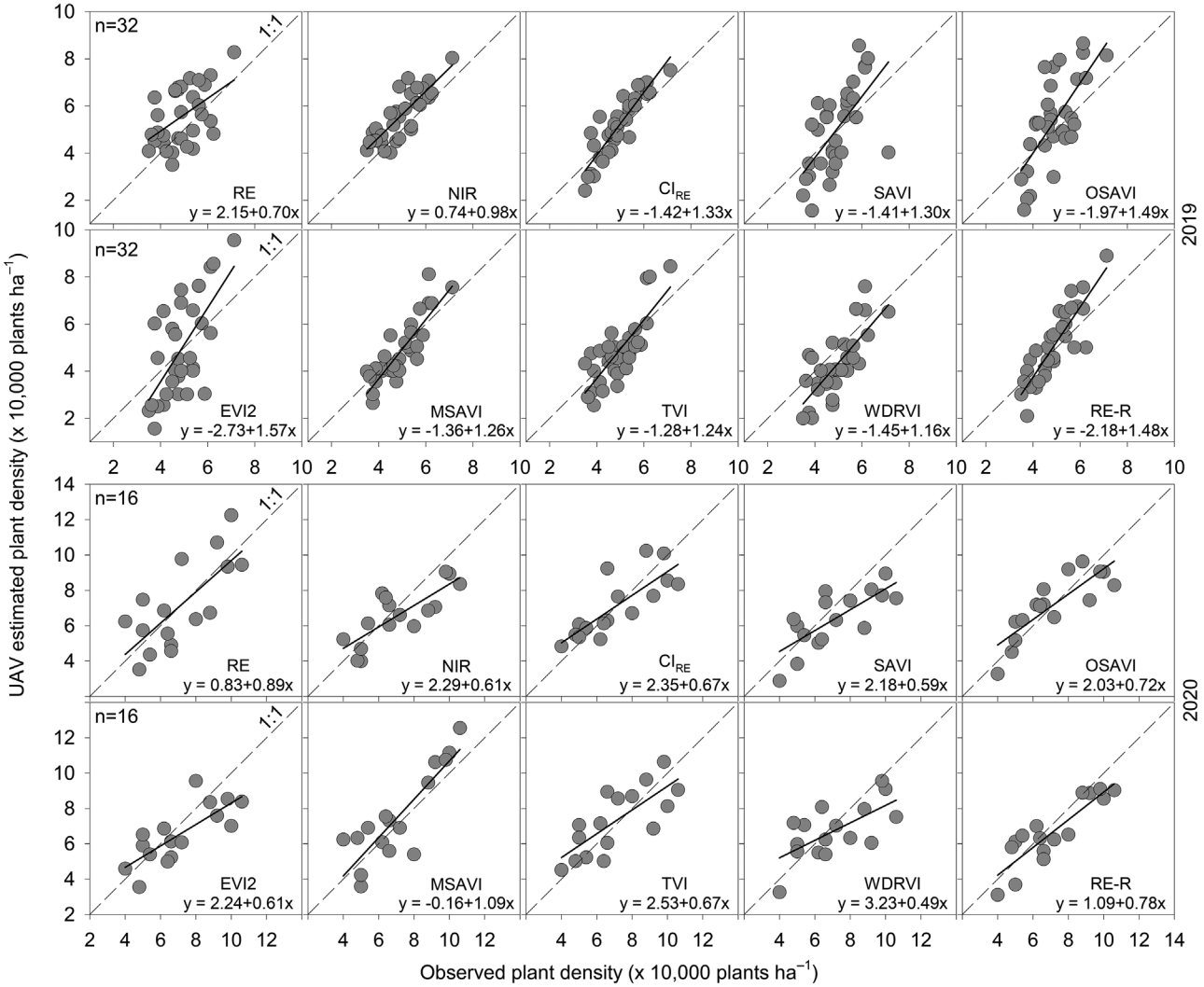

FIGURE 6 Relationship between observed and unmanned aerial vehicle (UAV) estimated plant density of cotton in 10 narrowband vegetation indices in (top two rows) 2019 and (bottom two rows) 2020. Vegetation indices are: RE, wavelength of red-edge; NIR, wavelength of near infrared; CI_{RE}, red-edge chlorophyll index; SAVI, soil adjusted vegetation index; OSAVI, optimized soil adjusted vegetation index; EVI2, two-band enhanced vegetation index; MSAVI, modified soil adjusted vegetation index; TVI, triangular vegetation index; WDRVI, wide dynamic range vegetation index; RE–R, red-edge minus red

3.6 | Evaluation of methods using independent datasets

The 21-Gun site had only cotton for the evaluation. Based on R^2, residual errors (RMSE and MAE), and IoA, ExG–ExR among the broadband and CI_{RE}, OSAVI, MSAVI, and RE–R among the narrowband indices were the final candidates chosen for evaluation, with an independent set of data obtained from the 21-Gun study (Table 7). The 21-Gun site did not have cover crop residue on the surface, and soil characteristics were slightly different from that of the LTAR site.

Performance of DSLR image analysis using ImageJ at 21-Gun was consistent with results obtained at the LTAR site, with comparable R^2 and IoA (Table 7). The SEE using ImageJ was also reduced to <4,500 plants ha^{-1}. Similarly, ImageJ estimated green canopy cover captured more than 90% of total variation within the LAI with low SEE. ImageJ showed the highest R^2 and lowest standard errors for both plant density and canopy cover prediction, relative to the UAV method. Selected VIs for UAV image analysis depict improvements in estimating density and cover (Table 7). Among them, soil adjusted VIs (MSAVI and OSAVI) led comparisons, providing confidence in robustness of the UAV method. Cohen's *k* of object-based segmentation was .80, .78, .93, .94, and .85 and *F* score was .76, .73, .90, .90, and .92 for ExG–ExR, CI_{RE}, MSAVI, OSAVI, and RE–R, respectively. Estimated canopy cover agreed with LAI, except for CI_{RE} (Table 7).

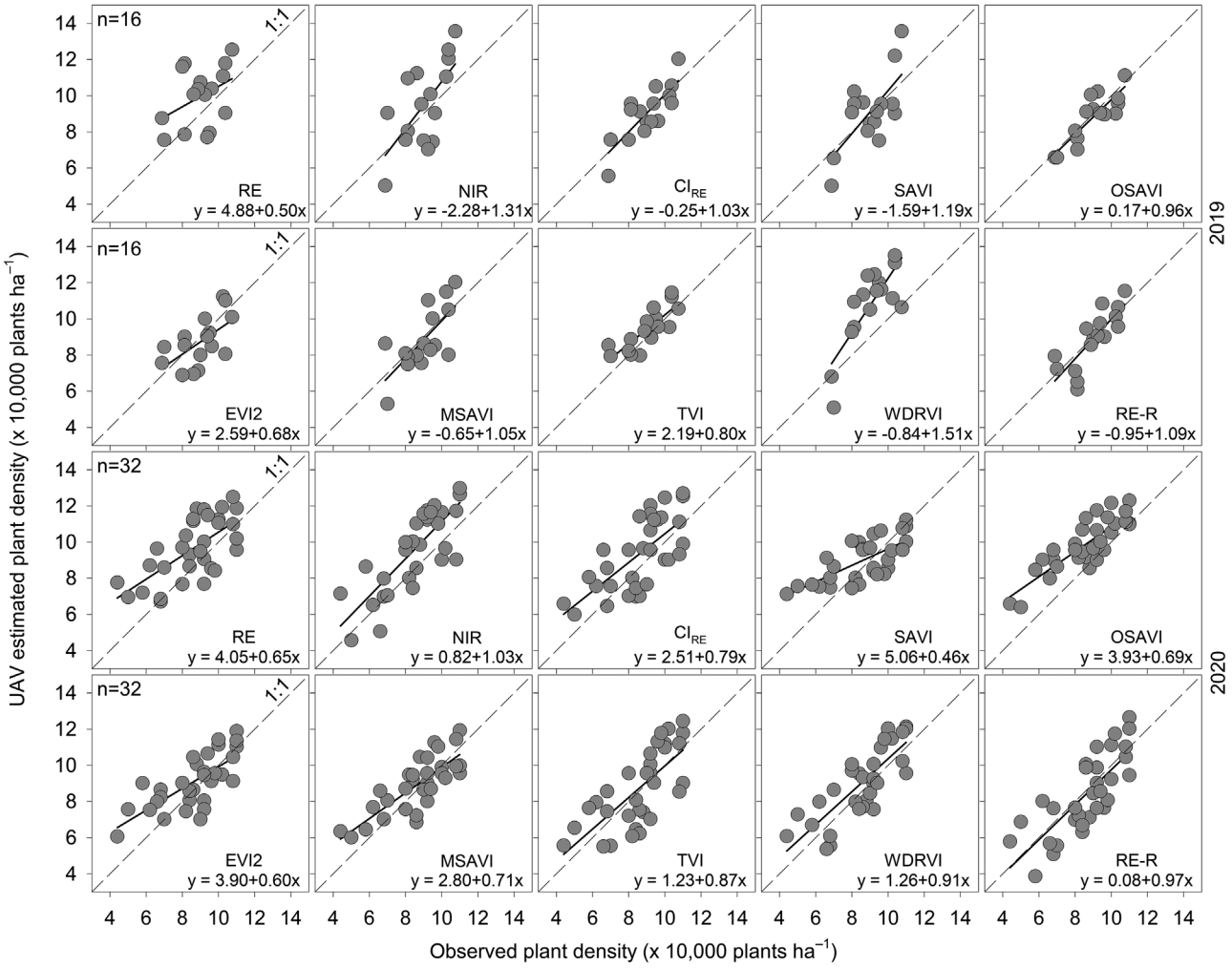

FIGURE 8 Relationship between observed and unmanned aerial vehicle (UAV) estimated plant density of sorghum in 10 narrowband vegetation indices in (top two rows) 2019 and (bottom two rows) 2020. Vegetation indices are: RE, wavelength of red-edge; NIR, wavelength of near infrared; CI_{RE}, red-edge chlorophyll index; SAVI, soil adjusted vegetation index; OSAVI, optimized soil adjusted vegetation index; EVI2, two-band enhanced vegetation index; MSAVI, modified soil adjusted vegetation index; TVI, triangular vegetation index; WDRVI, wide dynamic range vegetation index; RE–R, red-edge minus red

TABLE 6 Performance of red–green–blue (RGB) image interpretation using ImageJ in estimating plant density and vegetation cover of cotton and sorghum in 2019 and 2020

	Plant density				Cover vs. LAI	
Crop	R^2	RMSE	MAE	IoA	R^2	SEE
		——plants ha^{-1}——				—%—
Cotton						
2019	.79	7,214	6,040	.89	.82	1.10
2020	.90	6,461	5,617	.97	.78	1.98
Sorghum						
2019	.86	7,794	6,947	.91	.79	2.78
2020	.83	8,618	7,659	.91	.78	2.61

Note. IoA, index of agreement; LAI, leaf area index; MAE, mean absolute error; RMSE, root mean square error; SEE, standard error of estimate.

TABLE 7 Performance of red–green–blue (RGB) image interpretation using ImageJ in estimating plant density and vegetation cover of cotton in 2020 growing season

	Plant density				Cover vs. LAI	
Methods	R^2	RMSE	MAE	IoA	R^2	SEE
		——plants ha^{-1}——				
ImageJ	.93	4,308	3,610	.98	.92	1.16
UAV						
ExG–ExR	.77	8,059	7,714	.86	.77	2.29
CI_{RE}	.64	12,085	13,573	.80	.64	2.64
MSAVI	.85	6,185	5,194	.95	.85	1.55
OSAVI	.83	7,237	7,038	.93	.83	1.80
RE–R	.76	9,264	10,090	.92	.76	2.23

Note. IoA, index of agreement; LAI, leaf area index; MAE, mean absolute error; RMSE, root mean square error; SEE, standard error of estimate.

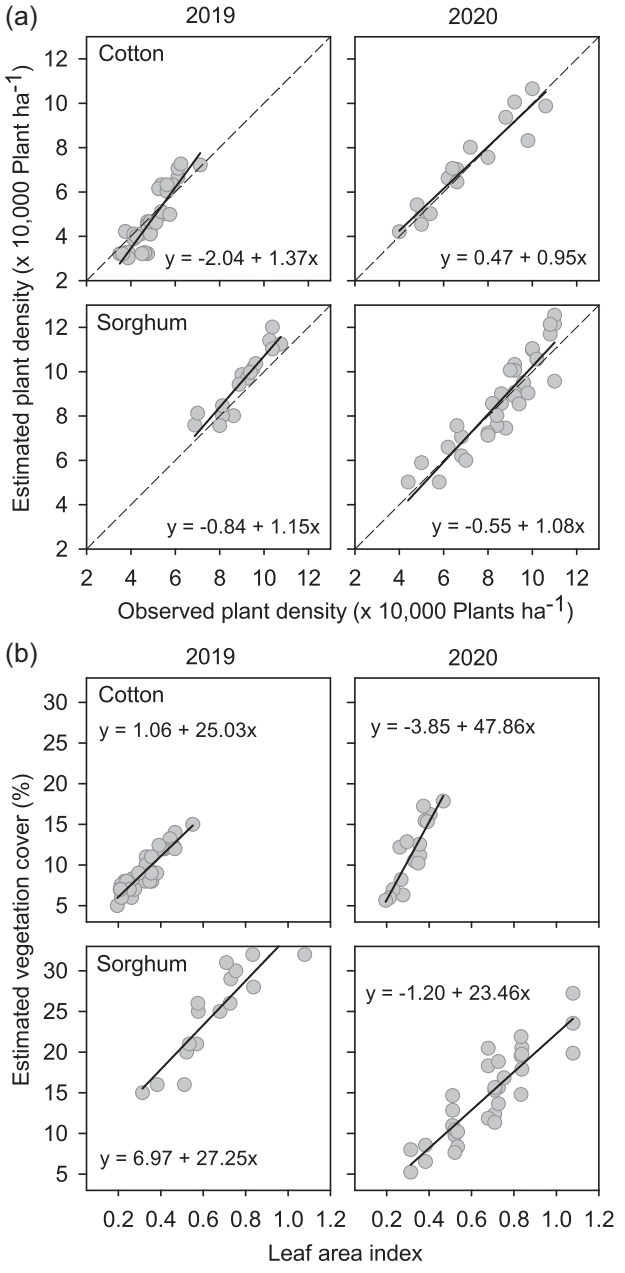

FIGURE 9 Relationship between estimated and observed plant density and between estimated canopy cover using ImageJ and leaf area index for cotton and sorghum in 2019 and 2020

TABLE 5 Unmanned aerial vehicle (UAV)-derived percentage vegetation cover of cotton and sorghum and R^2 of the linear relationship between the cover and leaf area index (LAI) for different vegetation indices (VIs) in 2019 and 2020

	Cotton				Sorghum			
	Cover		R^2		Cover		R^2	
VIs	2019	2020	2019	2020	2019	2020	2019	2020
	—%—				—%—			
Broadband								
RGB	8	2	.68	.51	20	13	.59	.46
ExG	12	6	.18	.46	22	15	.24	.55
ExR	12	10	.64	.48	22	20	.68	.60
ExG–ExR	12	17	.73	.83	23	21	.76	.73
NGRDI	8	8	.30	.61	23	10	.51	.44
Narrowband								
RE	13	27	.43	.61	30	38	.66	.59
NIR	11	20	.62	.70	22	20	.72	.67
CI_{RE}	11	14	.68	.81	20	26	.66	.63
SAVI	11	14	.65	.74	20	21	.65	.71
OSAVI	9	15	.30	.64	28	22	.63	.70
EVI2	10	11	.72	.63	19	20	.62	.58
MSAVI	11	16	.75	.82	22	14	.82	.76
TVI	11	17	.39	.44	27	19	.80	.66
WDRVI	10	16	.66	.55	22	25	.52	.64
RE–R	11	13	.55	.68	21	23	.79	.73

Note. CI_{RE}, red-edge chlorophyll index; EVI2, two-band enhanced vegetation index; ExG, excess green; ExR, excess red; ExG–ExR, excess green minus excess red; MSAVI, modified soil adjusted vegetation index; NDGRI, normalized green-red difference index; NIR, wavelength of near infrared; OSAVI, optimized soil adjusted vegetation index; RE, wavelength of red-edge; RE–R, red-edge minus red; RGB, red–green–blue; SAVI, soil adjusted vegetation index; TVI, triangular vegetation index; WDRVI, wide dynamic range vegetation index.

4 | DISCUSSION

4.1 | Effect of crop and surface characteristics

Cotton pixel segmentation was more accurate than that of sorghum. Glossy, wide, and bent sorghum leaves tended to illuminate more than hairy and dark green cotton leaves. These typical canopy attributes affected object-based segmentation in ArcGIS and binary thresholding in ImageJ. In ImageJ, cotton and sorghum residue in no-tillage plots produced a rough dark background hue, which led to imperfect binary color thresholding and creation of noise particles and voids on the leaf surface. Gap filling, dilation, and adjustment of size and circularity partially filled voids and removed noise particles including weeds and cover crop residue, but falsely recognized voids created due to leaf crisscrossing and erroneously added pixels to the total feature value. Leaf structure also affected estimation of plant density, as cumulative number of segments was not equal to number of plants for cotton. Two true leaves above the cotyledonary node were identified as two to four separate segments or plants by ImageJ due to differences in hue between leaf veins and blade. Such complexity necessitated use of a probabilistic model to find a suitable denominator to correct plant density. Although there were a few cases of merging two or more sorghum plants into a single clump in high-density areas, overall sorghum density was in line with total number of particles. Orientation of crop, soil illumination, solar angle and brightness,

crop height, camera angle, and color setting could also affect results (Xiong et al., 2019).

Average pixel value of the same crop from different treatments was significantly different for the same spectral band (Figure 5), and that justifies the use of color VI. Color VIs are considered less sensitive to lighting, as they can accentuate a color that may be useful in comparing plant greenness (Meyer & Neto, 2008). Among broadband indices, ExG–ExR had comparable accuracy to the narrowband indices, relative to ExG, ExR, and NGRDI. Utility of ExG–ExR for greater accuracy has been demonstrated (Zhang et al., 2017; Zhao et al., 2018). However, due to low spectral resolution, it was challenging to identify and segment plants from the background (Zhao et al., 2018). Jin et al. (2017) and Liu et al. (2017) advocated high-resolution multispectral images for improved accuracy under overlapped seedling conditions.

Soil adjusted VIs showed a significant reduction in noise across a wide range of vegetation and surface cover, including no-cover tilled plots. We obtained more reduction of first-order soil reflectance at L from 0.50 to 0.90, especially for no-cover plots due to high buffering of red reflectance variations, although Huete (1988) proposed using a soil-adjustment factor $L = 0.5$ (Table 2). The MSAVI has self-adjustable L (Qi et al., 1994) that increased dynamic range and further reduced soil background effects with high vegetation signal/soil noise ratio. Thus, we observed wide coverage of MSAVI from no-cover to cover crop and no-tillage to tilled plots. Another soil line vegetation index such as OSAVI (Haboudane et al., 2002; Rondeaux et al., 1996) also captured green cover and plant density variability with reduced background reflectance and enhanced sensitivity to greenness, although it did not provide a good estimate of cotton density in 2019. The merit of OSAVI and MSAVI is the nonmandatory use of soil line, which we believe is an advantage over original SAVI. Nevertheless, SAVIs that are insensitive to soil reflectance could be insensitive to variations in green canopy changes (Haboudane et al., 2002).

Change in red reflectance in relation to bare soil surface and variations from cover to no-cover surface potentially affected sensitivities of RE and NIR wavelengths, resulting in poor estimation of canopy cover and crop density. Sensitivity to chlorophyll is low for EVI2, but the index was highly responsive to canopy structural variations, including LAI and canopy architecture (Jiang et al., 2008). TVI also utilized green peak and NIR, based on chlorophyll absorption minima, making it highly sensitive for dense canopy (Xing et al., 2019). The NDVI-derived VIs (CI_{RE}, EVI2, and TVI) can only respond linearly to NIR reflectance when red reflectance is between 10 and 20% (Gitelson, 2004), but in our study, red reflectance ranged from 5 to 25% (data not shown) and may account for inconsistent results in dense sorghum stands and sparser cotton coverage. Reflectance variation between red and red-edge spectral region as proposed in this study provided a surprisingly good estimate of crop density and canopy cover. Red and red-edge had the opposite relationship when LAI was >0.25, with red-edge reflectance having more scatter than red ($R^2 = .46$) (Figure 5b). Xie et al. (2018) and Xing et al. (2019) confirmed that VIs with red-edge had scattered reflectance when the LAI was >3 and noted that combining red-edge with red and green reflectance improved chlorophyll sensitivity and relationship with LAI. Tables 4, 5, and 7 and Figures 4–8 depict improved accuracy and predictability of RE–R over the wavelength of RE and NIR for both cotton and sorghum.

With respect to choosing between broadband and narrowband indices, results suggest using soil-adjusted narrowband VIs to cover surface heterogeneity and a wide range of crop reflectance. Otherwise, use ExG–ExR if broadband RGB is the only option. This agrees with others that narrowband VIs were better for estimating crop attributes than broadband versions (Elvidge & Chen, 1995; Thenkabail et al., 2000; Zhao et al., 2007), although some research reported no difference between narrowband and broadband VIs (Broge & Leblanc, 2001; Broge & Mortensen, 2002).

4.2 | Limitation and use of UAV-based multispectral imagery and ImageJ

One of the major limitations of the quality of the UAV image analysis was the ground resolution that might affect segmentation accuracy and repeatability (Jin et al., 2017; Liu et al., 2017; Weber et al., 2006). The RMSE and MAE in our data could have been significantly reduced if the spatial resolution was higher. Low spatial resolution of images, especially at the narrowband spectrum may limit separation of adjacent seedlings due to progressive loss of detail around the object and feature values. Nevertheless, narrowband images contain higher spectral resolution or more bands than the broadband RGB images of high spatial resolutions (Kwan, 2019), so we could use more band ratios to detect an object of interest. The advantage of having narrowband images in our experiment was demonstrated by high segmentation accuracy of SAVIs.

Limited spectral choices pose challenges in selecting VIs due to low overall accuracy. For reliable implementation by land managers, segmentation must yield classification user accuracy >70% (Weber et al., 2006). Current VIs we used, fall in that range, but some of them did not maintain agreeable predictability of crop variables. Compared to UAV images, ultra-high-resolution DSLR images produced much better outcomes with ImageJ. However, it may take several hours to collect images from a quadrat at larger scales (Xiong et al., 2019). To collect 351 images, it took approximately 12 person-hours.

5 | CONCLUSIONS

ImageJ might be the best platform for image analysis based on overall accuracy of image classification and power in estimating cotton and sorghum density and canopy cover. However, ImageJ required acquisition of large numbers of DSLR images and intense image preprocessing. The ImageJ data engine was not sufficient to process multispectral datasets obtained using remote sensing tools. ArcGIS provided an opportunity to analyze UAV-based multispectral datasets using 15 broad and narrowband VIs, which were linearly related to the crop density and LAI. Among broadband VIs, ExG–ExR classified objects with more accurate scores and produced the smallest residual errors in estimating plant density and canopy cover, except for cotton in 2020. Narrowband VIs were more robust than broadband and consistently provided closer estimation across datasets obtained from both LTAR and 21-Gun sites. Most importantly, VIs related to soil line adjustment, that is, SAVI, MSAVI, and OSAVI captured the variability in plant density and LAI greater than wavelength of red-edge and NIR, TVI, and WDRVI. Interactions between red-edge and red reflectance (RE–R) also captured a wide range of surface characteristics. The combination of broadband color and multispectral images could provide a wide range of information from the crop canopy, which could be used to effectively assess cotton and sorghum stand establishment.

ACKNOWLEDGMENTS

We would like to thank technical and scientific personnel from the USDA-ARS National Sedimentation Laboratory, Oxford, MS; USDA-ARS Sustainable Water Management Research Unit; and USDA-ARS Crop Production Systems Research Unit, Stoneville, MS, for providing research facilities and support throughout the experiment. Partial funding was provided under Non-Assistance Cooperative Agreement no. 58-6066-0-045. This is a U.S. government work and not under copyright protection in the United States. This research was a contribution from the Long-Term Agroecosystem Research (LTAR) network. LTAR is supported by the United States Department of Agriculture.

AUTHOR CONTRIBUTIONS

Madhav Dhakal: Conceptualization; Data curation; Formal analysis; Investigation; Methodology; Software; Validation; Writing – original draft. Yanbo Huang: Data curation; Methodology; Resources; Software; Writing – review & editing. Martin A. Locke: Funding acquisition; Project administration; Resources; Supervision; Writing – review & editing. Krishna N. Reddy: Funding acquisition; Project administration; Resources; Supervision; Writing – review & editing. Matthew T Moore: Project administration; Resources; Supervision; Writing – review & editing. L. Jason Krutz: Methodology; Resources; Writing – review & editing. Drew Gholson: Resources. Rajen Bajgain: Resources; Writing – review & editing.

CONFLICT OF INTEREST

All authors have carefully reviewed, discussed, and agreed to the contents of the manuscript. The authors declare no conflict of interest.

ORCID

Madhav Dhakal https://orcid.org/0000-0003-3082-5225
Drew Gholson https://orcid.org/0000-0002-1060-2924

REFERENCES

Baxter, L. L., West, C. P., Brown, C. P., & Green, P. E. (2017). Comparing nondestructive sampling techniques for predicting forage mass in alfalfa-tall wheatgrass pasture. *Agronomy Journal*, *109*, 2097–2106. https://doi.org/10.2134/agronj2016.12.0738

Broge, N., & Leblanc, E. (2000). Comparing prediction power and stability of broadband and hyperspectral vegetation indices for estimation of green leaf area and canopy chlorophyll density. *Remote Sensing of Environment*, *76*, 156–172. https://doi.org/10.1016/S0034-4257(00)00197-8

Broge, N. H., & Leblanc, E. (2001). Comparing prediction power and stability of broadband and hyperspectral vegetation indices for estimation of green leaf area index and canopy chlorophyll density. *Remote Sensing of Environment*, *76*, 156–172. https://doi.org/10.1016/S0034-4257(00)00197-8

Broge, N. H., & Mortensen, J. V. (2002). Deriving green crop area index and canopy chlorophyll density of winter wheat from spectral reflectance data. *Remote Sensing of Environment*, *81*, 45–57. https://doi.org/10.1016/S0034-4257(01)00332-7

Chapman, S., Merz, T., Chan, A., Jackway, P., Hrabar, S., Dreccer, M., Holland, E., Zheng, B., Ling, T. J., & Jimenez-Berni, J. (2014). Pheno-Copter: A low-altitude, autonomous remote-sensing robotic helicopter for high-throughput field-based phenotyping. *Agronomy*, *4*, 279–301. https://doi.org/10.3390/agronomy4020279

Chu, T., Chen, R., Landvar, J. A., Maeda, M. M., Yang, C., & Starek, M. J. (2016). Cotton growth modeling and assessment using unmanned aircraft system visual-band imagery. *Journal of Applied Remote Sensing*, *10*, 036018. https://doi.org/10.1117/1.JRS.10.036018

Cook, R. D. (1977). Detection of influential observation in linear regression. *Technometrics*, *19*, 15–18. https://doi.org/10.2307/1268249

Czarnecki, Z. M. P., Samiappan, S., Wasson, L., McCurdy, J. D., Reynolds, D. B., Williams, W. P., & Moorhead, R. J. (2017). Applications of unmanned aerial vehicles in weed science. *Advances in Animal Biosciences*, *8*(2), 807–811. https://doi.org/10.1017/S2040470017001339

Dhakal, M., West C. P., & Villalobos C. (2019). Establishment and stand development of alfalfa interseeded into native grass mixture: Cultivar and row spacing effects. *Crop Science*, *59*, 2271–2279. https://doi.org/10.2135/cropsci2019.03.0156

Duan, T., Zhend, B. Y., Guo, W., Ninomiya, S., Guo, Y., & Chapman, S. C. (2017). Comparison of ground cover estimates from experiment plots in cotton, sorghum and sugarcane based on images and

ortho-mosaics captured by UAV. *Functional Plant Biology*, *44*, 169–183. https://doi.org/10.1071/FP16123

Elvidge, C. D., & Chen, Z. K. (1995). Comparison of broad-band and narrow-band red and near-infrared vegetation indexes. *Remote Sensing of Environment*, *54*(1), 38–48.

Ferguson, R., & Rundquist D. (2018). Remote sensing for site-specific crop management. In K. Shannon, D. E. Clay, & N. Kitchen (Eds.), *Precision agriculture basics*. ASA, CSSA, and SSSA.

Gitelson, A. A. (2004). Wide dynamic range vegetation index for remote quantification of biophysical characteristics of vegetation. *Journal of Plant Physiology*, *161*, 165–173. https://doi.org/10.1078/0176-1617-01176

Gitelson, A. A., & Merzlyak, M. N. (1994). Quantitative estimation of chlorophyll using reflectance spectra. *Journal of Photochemistry Photobiology B*, *22*, 247–252. https://doi.org/10.1016/1011-1344(93)06963-4

Gitelson, A. A., Stark, R., Grits, U., Rundquist, D. C., Kaufman, Y. J., & Derry, D. (2002). Vegetation and soil lines in visible spectral space: A concept and technique for remote estimation of vegetation fraction. *International Journal of Remote Sensing*, *23*, 2537–2562. https://doi.org/10.1080/01431160110107806

Haboudane, D., Miller, J. R., Tremblay, N., Zarco-Tejada, P. J., & Dextraze, L. (2002). Integrated narrow-band vegetation indices for prediction of crop chlorophyll content for application to precision agriculture. *Remote Sensing of Environment*, *81*, 416-426. https://doi.org/10.1016/S0034-4257(02)00018-4

Huete, A. R. (1988). A soil-adjusted vegetation index (SAVI). *Remote Sensing of Environment*, *25*, 295–309. https://doi.org/10.1016/0034-4257(88)90106-X

Jiang, Z., Huete, A. R., Didan, K., & Miura, T. (2008). Development of a two-band Enhanced Vegetation Index without a blue band. *Remote Sensing of Environment*, *112*, 3833–3845, https://doi.org/10.1016/j.rse.2008.06.006

Jin, X., Liu, S., Baret, F., Hemerlé, M., & Comar, A. (2017). Estimates of plant density of wheat crops at emergence from very low altitude UAV imagery. *Remote Sensing of Environment*, *198*, 105–114. https://doi.org/10.1016/j.rse.2017.06.007

Koh, J. C. O., Hayden, M., Daetwler, H., & Kant, S. (2019). Estimation of crop plant density at early mixed growth stages using UAV imagery. *Plant Methods*, *15*, 64. https://doi.org/10.1186/s13007-019-0449-1

Kwan, C. (2019). Methods and challenges using multispectral and hyperspectral images for practical change detection applications. *Information*, *10*(11), 353. https://doi.org/10.3390/info10110353

Li, B., Xu, X., Han, J., Zhang, L., Bian, C., Jin, L., & Liu, J. (2019). The estimation of crop emergence in potatoes by UAV RGB imagery. *Plant Methods*, *15*, 15. https://doi.org/10.1186/s13007-019-0399-7

Li, B., Xu, X., Zhang, L., Han, J., Biana, C., Li, G., Liu, J., & Jin, L. (2020). Above-ground biomass estimation and yield prediction in potato by using UAV-based RGB and hyperspectral imaging. *ISPRS Journal of Photogrammetry and Remote Sensing*, *162*, 161–172. https://doi.org/10.1016/j.isprsjprs.2020.02.013

Liu, S. Y., Baret, F., Andrieu, B., Burger, P., & Hemmerlé, M. (2017). Estimation of wheat plant density at early stages using high resolution imagery. *Frontiers in Plant Science*, *8*, 739. https://doi.org/10.3389/fpls.2017.00739

Liu, J., Pattry, E., & Jego, G. (2012). Assessment of vegetation indices for regional crop green LAI estimation from Landsat images over multiple growing seasons. *Remote Sensing of Environment*, *123*, 347–358. https://doi.org/10.1016/j.rse.2012.04.002

McHugh, M. L. (2012). Interrater reliability: The kappa statistic. *Biochemia Medica*, *22*, 276–282. https://doi.org/10.11613/bm.2012.031. PMC3900052.PMID 23092060.

Meyer, G. E., & Neto, J. C. (2008). Verification of color vegetation indices for automated crop imaging applications. *Computers and Electronics in Agriculture*, *63*, 282–293. https://doi.org/10.1016/j.compag.2008.03.009

Portz, G., Molin, J. P., & Jasper, J. (2012). Active crop sensor to detect variability of nitrogen supply and biomass on sugarcane fields. *Precision Agriculture*, *13*, 33–44. https://doi.org/10.1007/s11119-011-9243-4

Qi, J., Chehbouni, A., Huete, A. R., Kerr, Y. H., & Sorooshian, S. (1994). A modified soil adjusted vegetation index. *Remote Sensing of Environment*, *48*, 119–126. https://doi.org/10.1016/0034-4257(94)90134-1

Rondeaux, G., Steven M., & Baret F. (1996). Optimization of soil-adjusted vegetation indices. *Remote Sensing of Environment*, *55*, 95–107. https://doi.org/10.1016/0034-4257(95)00186-7

Sasaki, Y. (2007). *The truth of the F-measure*. https://www.cs.odu.edu/~mukka/cs795sum09dm/Lecturenotes/Day3/F-measure-YS-26Oct07.pdf

Stroup, W. W. (2015). Rethinking the analysis of non-normal data in plant and soil science. *Agronomy Journal*, *107*, 811–827. https://doi.org/10.2134/agronj2013.0342

Thenkabail, P., Smith, R. B., & De Pauw, E. (2000). Hyperspectral vegetation indices and their relationships with agricultural crop characteristics. *Remote Sensing of Environment*, *71*, 158–182. https://doi.org/10.1016/S0034-4257(99)00067-X

Thenkabail, P., Smith, R. B., & Pauw, E. D. (2002). Evaluation of narrowband and broadband vegetation indices for determining optimal hyperspectral wavebands for agricultural crop characterization. *Photogramming Engineering Remote Sensing*, *68*, 607–621.

Vapnik, V. (2013). *The nature of statistical learning theory*. Springer Science & Business Media.

Weber, K. T., Glenn, N. F., Mundt, J. T., & Gokhale, B. (2006). A comparison between multispectral and hyperspectral platforms for early detection of leafy spurge in Southeastern Idaho. In K. T. Weber (Ed.), *Detection, prediction, impact, and management of invasive plants using GIS* (pp. 185—196). Idaho State University, GIS Training and Research Center.

Willmott, C. J. (1982). Some comments on the evaluation of model performance. *Bulletin of the American Meteorological Society*, *11*, 1303–1313. https://doi.org/10.1175/1520-0477(1982)063⟨1309:SCOTEO⟩2.0.CO;2

Xie, Q., Dash, J., Huang, W., Peng, D., Qin, Q., Mortimer, H., Casa, R., Pignatti, S., Laneve, G., Pascucci, S., Dong, Y., & Ye, H. (2018). Vegetation indices combining the red and red-edge spectral information for leaf area index retrieval. *IEEE Journal of Selected Topics Applied Earth Observation Remote Sensing*, *11*(5), 1482–1493. https://doi.org/10.1109/JSTARS.2018.2813281

Xing, N., Huang, W., Xie, Q., Shi, Y., Ye, H., Dong, Y., Wu, M., Sun, G., & Jiao, Q. (2019). A transformed triangular vegetation index for estimating winter wheat leaf area index. *Remote Sensing*, *12*, 16. https://doi.org/10.3390/rs12010016

Xiong, Y. D., West, C. P., Brown, C. P., & Green, P. E. (2019). Digital image analysis of old-world bluestem cover to estimate canopy development. *Agronomy Journal*, *111*, 1247–1253. https://doi.org/10.2134/agronj2018.08.0502

Xue, J., & Su, B. (2017). Significant remote sensing vegetation indices: A review of developments and applications. *Hindawi Journal Sensors*, *2017*, 1–17. https://doi.org/10.1155/2017/1353691

Zandbergen, P. A. (2013). *Python scripting for ArcGIS*. ESRI Press.

Zhang, J., Yang, C., Zhao, B., Song, H., Clint Hoffmann, W., Shi, Y., Zhang, D., & Zhang, G. (2017). Crop classification and LAI estimation using original and resolution reduced images from two consumer-grade cameras. *Remote Sensing*, *9*, 1054. https://doi.org/10.3390/rs9101054

Zhao, D., Huang, L., Li, J., & Qi, J. (2007). A comparative analysis of broadband and narrowband derived vegetation indices in predicting LAI and CCD of a cotton canopy. *ISPRS Journal of Photogrammetry Remote Sensing*, *62*, 25–33. https://doi.org/10.1016/j.isprsjprs.2007.01.003

Zhao, B., Zhang, J., Yang, C., Zhou, G., Ding, Y., Shi, Y., Zhang, D., Xie, J., & Liao, Q. (2018). Rapeseed seedling stand counting and seeding performance evaluation at two early growth stages based on unmanned aerial vehicle imagery. *Frontiers in Plant Science*, *9*, 1362. https://doi.org/10.3389/fpls.2018.01362

How to cite this article: Dhakal, M., Huang, Y., Locke, M. A., Reddy, K. N., Moore, M. T., Krutz, L. J., Gholson, D., & Bajgain, R. (2022). Cotton and sorghum stand assessment of cotton and sorghum stand establishment using UAV-based multispectral and DSLR-based RGB imagery. *Agrosystems, Geosciences & Environment*, *5,* e20247. https://doi.org/10.1002/agg2.20247